sensors

MDPI

Article

Indirect Thermographic Measurement of the Temperature of a Transistor Die during Pulse Operation

Arkadiusz Hulewicz [1,*], Krzysztof Dziarski [2] and Łukasz Drużyński [2]

[1] Institute of Electrical Engineering and Electronics, Poznan University of Technology, Piotrowo 3A, 60-965 Poznan, Poland
[2] Institute of Electric Power Engineering, Poznan University of Technology, Piotrowo 3A, 60-965 Poznan, Poland; krzysztof.dziarski@put.poznan.pl (K.D.); lukasz.druzynski@put.poznan.pl (Ł.D.)
* Correspondence: arkadiusz.hulewicz@put.poznan.pl

Abstract: This paper presents aspects related to the indirect thermographic measurement of a C2M0280120D transistor in pulse mode. The tested transistor was made on the basis of silicon carbide and is commonly used in many applications. During the research, the pulse frequency was varied from 1 kHz to 800 kHz. The transistor case temperature was measured using a Flir E50 thermographic camera and a Pt1000 sensor. The transistor die temperature was determined based on the voltage drop on the body diode and the known characteristics between the voltage drop on the diode and the temperature of the die. The research was carried out in accordance with the presented measuring standards and maintaining the described conditions. The differences between the transistor case temperature and the transistor die temperature were also determined based on simulation work performed in Solidworks 2020 SP05. For this purpose, a three-dimensional model of the C2M0280120D transistor was created and the materials used in this model were selected; the methodology for selecting the model parameters is discussed. The largest recorded difference between the case temperature and the junction temperature was 27.3 °C. The use of a thermographic camera allows the transistor's temperature to be determined without the risk of electric shock. As a result, it will be possible to control the C2M0280120D transistor in such a way so as not to damage it and to optimally select its operating point.

Keywords: thermography; C2M0280120D; transistor; switching; thermal modelling; solidworks

Citation: Hulewicz, A.; Dziarski, K.; Drużyński, Ł. Indirect Thermographic Measurement of the Temperature of a Transistor Die during Pulse Operation. *Sensors* **2024**, *24*, 6452. https://doi.org/10.3390/s24196452

Academic Editors: Grzegorz Peruń and Tangbin Xia

Received: 11 August 2024
Revised: 1 October 2024
Accepted: 3 October 2024
Published: 6 October 2024

1. Introduction

Transistors are among the electronic components from which electronic devices are built [1]. They consist of a die placed on a base plate made of a well-conducting metal, which, in many cases, is copper. The die is encapsulated inside epoxy resin, and connections to die are possible using leads, commonly called "legs", which are often made of the same material as the base plate. Only one of the leads is directly attached to the base plate. The remaining two leads are placed in the epoxy resin and connected to the die using thin bond wires. The parts of the base plate and leads that are not placed under the epoxy resin layer are covered with a thin layer of tin [2,3]. The dimensions of the base plate, leads, and the epoxy resin layer depend on the type of case used; the most commonly used cases are TO 220 and TO 247. The dimensions of the electronic cases are standardized [4]. In the remainder of this article, the term "transistor" should be understood together with the case in which it is placed.

The most popular materials from which transistor dies are made include silicon (Si), silicon carbide (SiC), and gallium nitride (GaN). Transistors made of these materials differ in their properties [5]. Electronic components made on the basis of silicon reach the limit operating parameters resulting from the theoretical limitations of the material used. For this reason, electronic components based on SiC and GaN materials, called wide band gap

(WBG) semiconductors, are becoming more and more popular. They feature better electrical, mechanical, and thermal properties than the electronic components made on the basis of Si. Replacing Si with WBG semiconductors increases the breakdown voltages, operating temperatures, and switching frequency and reduces switching losses [6]. Elements made on the basis of SiC deserve special attention. Compared to Si elements, those made on the basis of SiC have higher breakdown voltage values and higher thermal conductivity [7]. Another feature of this type of semiconductor is low ON-resistance [8].

Metal oxide semiconductor field effect transistors (MOSFETs) made on the basis of SiC are used in the construction of high conversion ratio converters (HCRCs) [9], traction converters [10], wind turbine converters [11], motor drives for electric vehicles [12], and DC–DC step-up converters [13]. The operational reliability of these devices is related to the operational reliability of the SiC MOSFETs placed inside them [14]. Due to the construction of the die area and the width of the gate oxide, they are susceptible to transient-overloading or short-circuit events [15]. Other examples of SiC MOSFET damage are related to long-term exposure to high temperature, which can cause interlayer dielectric erosion, electrode delamination, gate-oxide breakdown [16], and bond-wire lift-off and solder cracks [17,18].

The temperature value of SiC MOSFETs depends, among other things, on their switching frequency [19]. In turn, the switching frequency depends on the operating characteristics of the device in which the transistor is placed and on its energy efficiency [20]. A good example is the converter. In high-power converters, lower switching frequencies are often used to minimize switching losses and increase energy efficiency [21]. In turn, in low-power converters, higher switching frequencies are usually used, which may lead to smaller converter sizes and better regulation [22]. The higher the switching frequency is, the shorter is the switching time of SiC-based MOSFETs. During switching, rapid changes in voltage and current occur, which leads to power losses and heat generation. Therefore, the switching frequency has a direct impact on heat generation in the transistor [23].

The switching frequency of a SiC MOSFET affects the temperature of its die. In turn, the operation of the die at excessively high temperature may damage the transistor. For this reason, it is necessary to monitor the die temperature of the transistor, T_j. In the literature, is possible to find three groups of methods that make this possible: electrical, contact, and non-contact methods [24].

Electrical methods use a selected parameter whose value depends on T_j. This parameter is called the temperature-sensitive parameter (TSP) [25]. An example of a TSP that is used to determine the die temperature of a transistor is the drop voltage across the body diode. Knowing the relationship between TSP and T_j, it is possible to determine the T_j value based on the measured TSP value. The relationship between TSP and T_j is individual for each transistor. Additionally, its determination requires removing the transistor from the device in which it was installed and placing it in the measurement system. For this reason, this method is not suitable for real-time monitoring of T_j values [26].

Contact methods involve applying a temperature sensor to the transistor package (also called a 'case' in the literature) or directly to the die transistor. There is thermal resistance of an unknown value between the temperature sensor case and the transistor case (or die). Additionally, touching the transistor (or die) case with the temperature sensor causes a local disturbance of the temperature distribution. Part of the transistor case is made of metal; therefore, incorrect application of the temperature sensor (especially when placed in a metal case) may cause electric shock [27].

Non-contact methods are based on the absorption of infrared radiation emitted from the surface of the transistor case (indirect non-contact method) or through the transistor die (direct non-contact method). One of these methods is infrared thermography, which is considered safe, as it poses no risk of electric shock (e.g., as a result of touching a metal temperature sensor based on a plate or a radiator to which a transistor is attached). The direct method requires opening the transistor case. It is difficult to close the opened case. For this reason, it is not suitable for real-time application. The use of the indirect non-contact method consists of two steps: measuring the temperature of the transistor case (T_c) and

determining the difference between T_c and T_j. T_c can be measured using a pyrometer and a thermographic camera. The use of a thermographic camera makes it possible to determine the temperature distribution on the surface of the transistor case. The differences between T_c and T_j can be determined using the finite element method. Knowing the value of the thermographic measurement of the temperature of the transistor case and the relationship between T_c and T_j, it is possible to determine the value of T_j in real time [28,29].

After analyzing the available sources, no studies were found on the indirect thermographic temperature measurement of a SiC MOSFET, the temperature of which increases due to the increase in the switching frequency. For this reason, it was decided to undertake research that would result in the development of a method enabling the indirect thermographic measurement of the SiC MOSFET die temperature and monitoring that temperature at variable switching frequencies.

Section 2 describes the tested SiC MOSFET, the methodology, and the measurement system; Section 3 describes the obtained results of the work; Section 4 contains a discussion; and Section 5 presents conclusions.

2. Tested Transistor, Methodology, and Measurement System

The indirect thermographic measurement of the transistor temperature die consists of two parts. The first part consists of performing a thermographic measurement of the transistor case temperature, T_c. The second part consists of determining the transistor die value T_j using simulation work. The method of performing a thermographic measurement of T_c is described in Section 2.1. The value of T_{Pt1000}, which is used to verify the T_c value, is also determined and described in Section 2.1. The method used to determine the T_j value based on simulation work is described in Section 2.2. The method for determining the T_{jd} value, which is used to verify the T_j value (determined based on simulation work), is also described in Section 2.2. The algorithm for the procedure is presented in Figure 1.

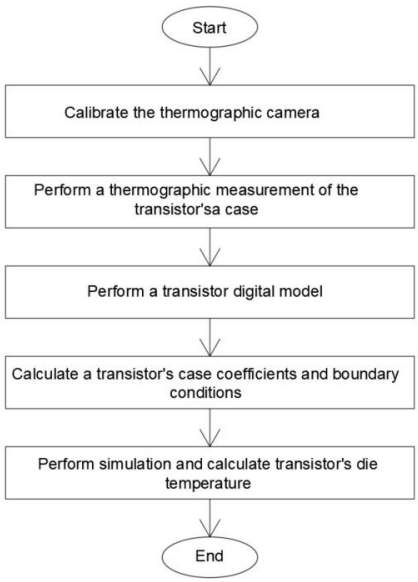

Figure 1. Algorithm for performing indirect thermographic temperature measurements of a transistor.

2.1. Tested Transistor and Measurement System

The model C2M0280120D (Cree Inc., Durham, NC, USA) transistor was selected for testing. This transistor is described by the following parameters: V_{DSmax} = 1200 V (for V_{GS} = 0 V, I_D = 100 µA), V_{GSmax} = −10/+25 V, I_D = 10 A (for V_{GS} = 20 V, T_c = 25 °C), I_D = 6 A (for V_{GS} = 20 V, T_c = 100 °C), and I_{Dpulse} = 20A. The external dimensions of the transistor and schematics are shown in Figure 2. Three randomly selected C2M0280120D transistors from the same series were selected to carry out the work.

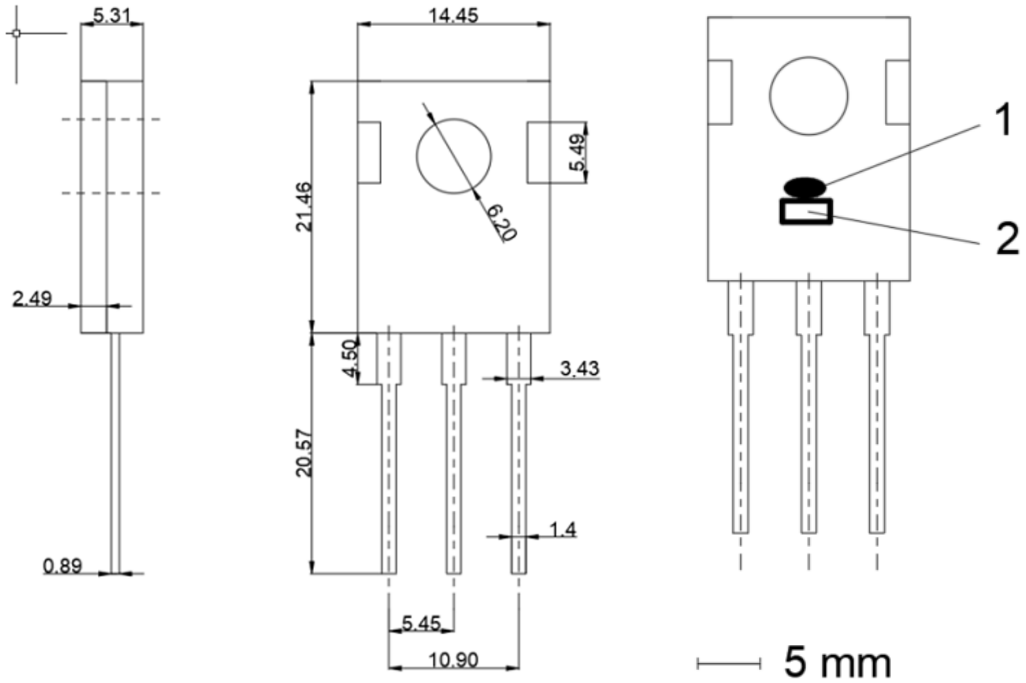

Figure 2. (**a**) External dimensions of transistor model C2M0280120D in a TO 247 case. (**b**) Schematic of C2M0280120D in a TO 247 case. A marker was painted on the case using Velvet Coating 811-21 paint (1) and a Pt1000 sensor was glued onto the case (2).

Pt1000 sensors in an SMD 6203 case (Reichelt electronics GmbH & Co. KG, Sande, Germany) were glued to the case of each transistor [30]. For this purpose, WLK 5 glue with a known thermal conductivity value of k = 0.836 W/mK (Fischer Elektronik GmbH & Co. KG, Lüdenscheid, Germany) was used [31]. Additionally, next to the Pt1000 sensor, a measurement marker was painted on the transistor case. Velvet Coating 811-21 (Nextel, Hamburg, Germany) paint was used for this purpose with a known emissivity coefficient value ε ranging from 0.970 to 0.975 for temperatures within the range from –36 °C to 82 °C. The uncertainty with which the emissivity coefficient value was determined was 0.004 [32].

The transistor prepared in this way was placed in a station where the measuring device was a Flir E50 Thermographic Camera (Flir, Wilsonville, OR, USA) [33]. The selected Flir E50 thermographic camera was equipped with a matrix from an uncooled IR detector (7.5–13 µm) with a resolution of 240 × 180 pixels and an instantaneous field of view (IFOV) value of 1.82 mrad. The noise equivalent differential temperature (NEDT) value of this camera was 50 mK. An additional Close-up 2× lens (T197214, Flir, Wilsonville, OR, USA) was attached to the camera lens [34]. As a consequence, it was possible to obtain an IFOV value of 67 µm for the above-mentioned detector array (240 × 180 pixels) (thermographic camera with the additional lens). Before starting the work, the correctness of the indications of the camera used was verified using the IRS Calilux thermographic camera calibration standard (AT—Automation Technology GmbH, Bad Oldesloe, Germany) [35].

The thermographic camera prepared in this way was placed together with the tested C2M0280120D transistor in a chamber made of plexiglass. The external dimensions of the chamber were 45 cm × 35 cm × 35 cm. The internal dimensions of the chamber were 40 cm × 30 cm × 30 cm. The difference resulted from two reasons: the thickness of the plexiglass used (3 mm) and the thickness of the material (black foam made of polyurethane) lining the internal walls of the chamber. The foam used is characterized by porous structure, and every single pore of the foam resembles the black body cavity model. As a consequence, the material used was characterized by having a high emissivity factor ε = 0.95 [36].

The distance *d* between the tested transistor and the additional lens was adjusted using a stepper motor. In turn, the stepper motor was controlled using a Siemens S7-1200 PLC controller (Siemens AG, Munich, Germany) [37]. A block diagram of the constructed stand is shown in Figure 3.

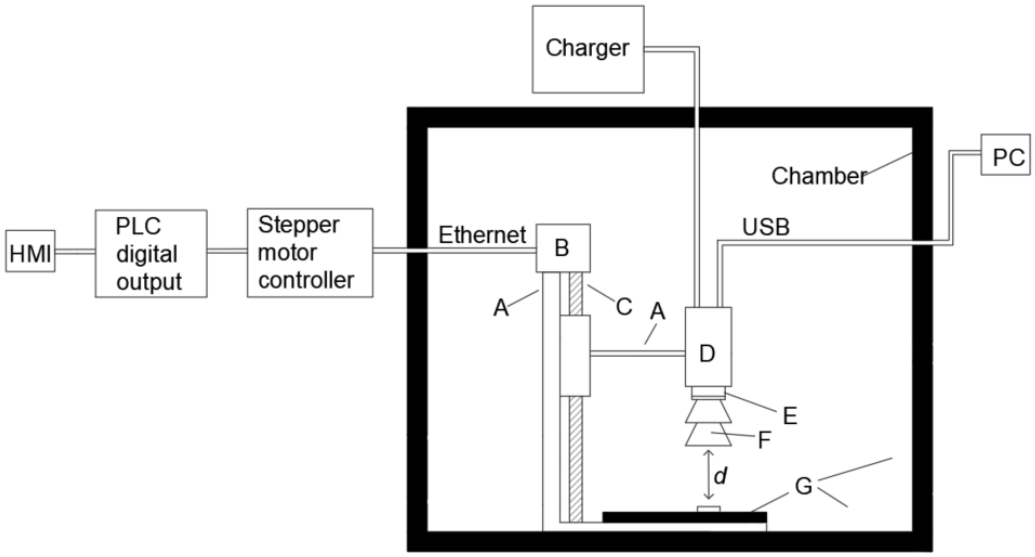

Figure 3. Thermographic camera and observed transistor placed in the prepared chamber. A—stand, B—stepper motor, C—screw, D—thermographic camera, E—thermographic camera lens, F—additional thermographic camera lens, G—polyurethane foam, d—distance between the tested transistor and the additional lens.

The observed transistor was connected to a circuit that allowed its switching frequency to be changed. The circuit diagram is shown in Figure 4. In this circuit, the transistor *T1* was turned on by the generator *G1* for 20 s. As a result, the load current I_{DS} flowed through the tested transistor. During this time, the voltage drop between the drain and the source V_{DS} was measured using an Agilent 34401A voltmeter. In the next step, the same generator *G1* turned on transistor *T2*, allowing the flow of the measuring current I_{di} for 200 ms. This operation allowed estimating the die temperature based on the automatic measurement of the drop voltage V_{fd} on the diode and the known characteristic between the drop voltage value and the die temperature. During the entire testing process, the tested transistor (DUT) was pulse-controlled using the *G2* generator with a PWM waveform with a duty cycle of 50% and a frequency in the range from 1 kHz to 50 kHz.

The case of the tested transistor, in which the switching frequency was changed, was observed using a thermographic camera. During the tests, first, for a given value of the current I_{DS} flowing through the die and a given switching frequency f_T, the temperature of the case (T_c) was measured using a thermographic camera. We then waited until its value increased and stabilized at a specified level. When it was found that the T_c value had stabilized, its thermographic measurement was performed. At the same time, T_c was measured using a Pt1000 sensor, which was glued to the case near the thermographic measurement point (Figure 2). After the measurement was performed, the switching frequency f_T of the transistor was changed for the same I_D current value. The f_T setting was changed for selected values, ranging from 1 kHz to 800 kHz.

2.2. Finite Element Analysis and Measurement of Die Temperature

The relationship between T_c and T_j was determined using finite element analysis (FEA), which is a numerical method used to solve problems in engineering and mathematical physics [38]. The software applied in the work performed was Solidworks 2020 SP05 (Dassault Systèmes, Vélizy-Villacoublay, France), which uses FEA, and the simulation was completed with the use of this software.

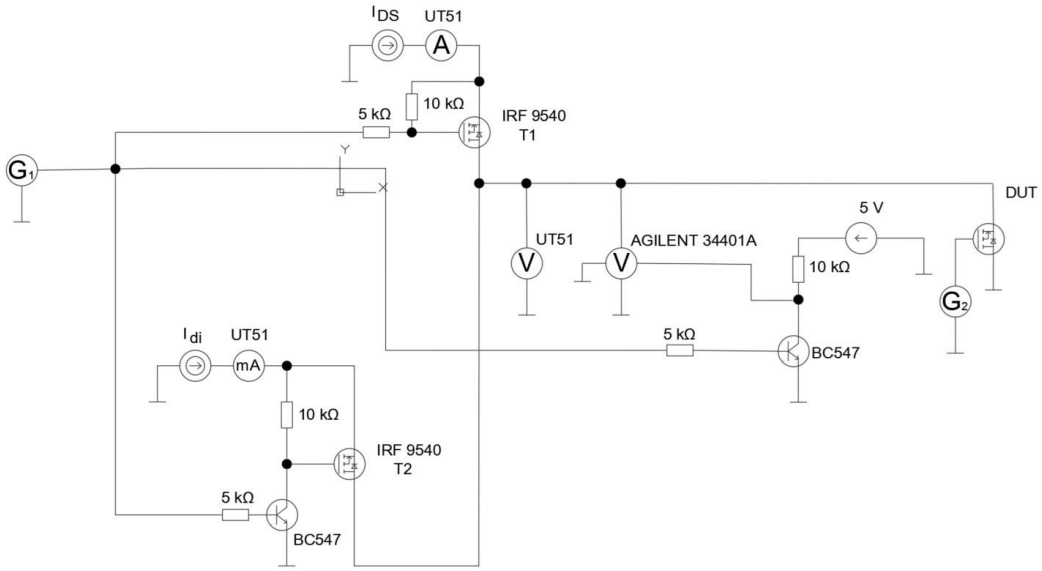

Figure 4. Diagram of the circuit enabling the evaluation of the influence of the switching frequency changes of the transistor on the temperature of its die. DUT—device under test, i.e., the tested transistor.

The simulation could be carried out after the transistor model had been constructed. Making the model required knowledge of its structure and internal dimensions. In order to determine these, the case of the tested transistor was opened and its interior was measured. For this purpose, a microscope equipped with a Cam 3.3 MP camera (Motic, Xiamen, China) was used. The microscope with the camera was calibrated using a special calibration glass. Based on the measurements taken, a three-dimensional model of the tested transistor was created. The model was created in Solidworks 2020 SP05 software. The created model and internal dimensions of the tested transistor C2M0280120D are shown in Figure 5.

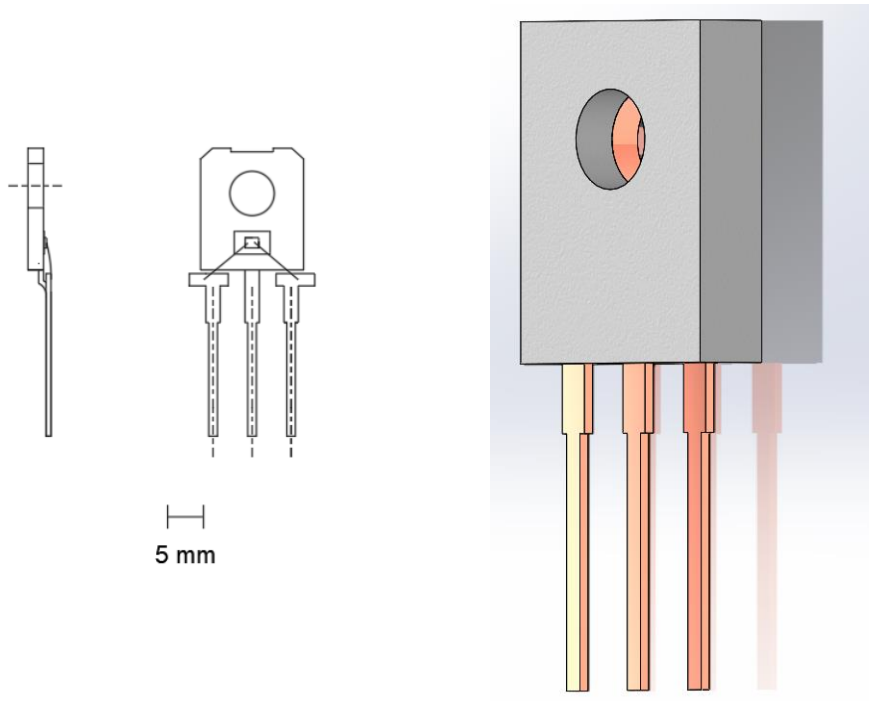

(**a**) (**b**)

Figure 5. (**a**) Internal dimensions (see Figure 2 for details) and (**b**) three-dimensional model of the C2M0280120D transistor.

After creating the model, all of its elements were assigned the material from which it was made, along with the thermal conductivity values k. Next, the simulation was started in the Solidworks 2020 SP05 environment. In the initial stage, we checked whether the temperature distribution (measured at the surface) changes after removing individual parts of the model (e.g., leads). The temperature distribution was also checked, depending on the given mesh size. After simplifying the model and selecting the mesh size, it was possible to determine the T_j value based on the simulation work.

The die temperature (T_j) of the tested transistors obtained as a result of simulation work was verified for the same conditions using the electrical method. In order to perform a reliable temperature measurement of the die using the electrical method, it was necessary to select the appropriate temperature-sensitive parameter (TSP). The voltage drop V_{fd} across the body diode was chosen as the TSP. In order to use the TSP to determine the T_j value, the relationship $T_j = f(V_{fd})$ had to be determined. For this reason, a measuring system was designed, the main element of which was a climatic chamber. The chamber used allowed for changing the temperature T_a inside it. The T_a value was changed in the range from 20 °C to 180 °C. Additionally, a Pt1000 sensor was placed inside the chamber, which was used to measure the temperature there. The sensor was connected in a four-wire circuit for measuring resistance using the technical method. A current of 100 µA flowed through the sensor.

In order to determine the relationship $T_j = f(V_{fd})$, three tested transistors were placed inside the described chamber. They were connected in such a way that the current I_{di} (I_{di} = 100 mA) forcing the voltage drop V_{fd} on the body diode flowed through all diodes of the tested transistors (the body diodes of the three transistors were connected in series). The measurement setup is shown in Figure 6. The V_{fd} values of all tested transistors were measured using an Agilent 34401A multimeter (Agilent, Santa Clara, CA, USA) [39]. The measurement was performed for a given temperature T_a at the moment when the V_{fd} voltage value stabilized. The constant values of the V_{fd} voltage in time indicated that the temperature T_a set in the chamber was equal to the die temperature T_j of the transistors located in this chamber. In turn, the voltage drop V_{Pt1000} on the Pt1000 sensor was measured using a UT51 multimeter (UNI-T, Dongguan City, China) [40].

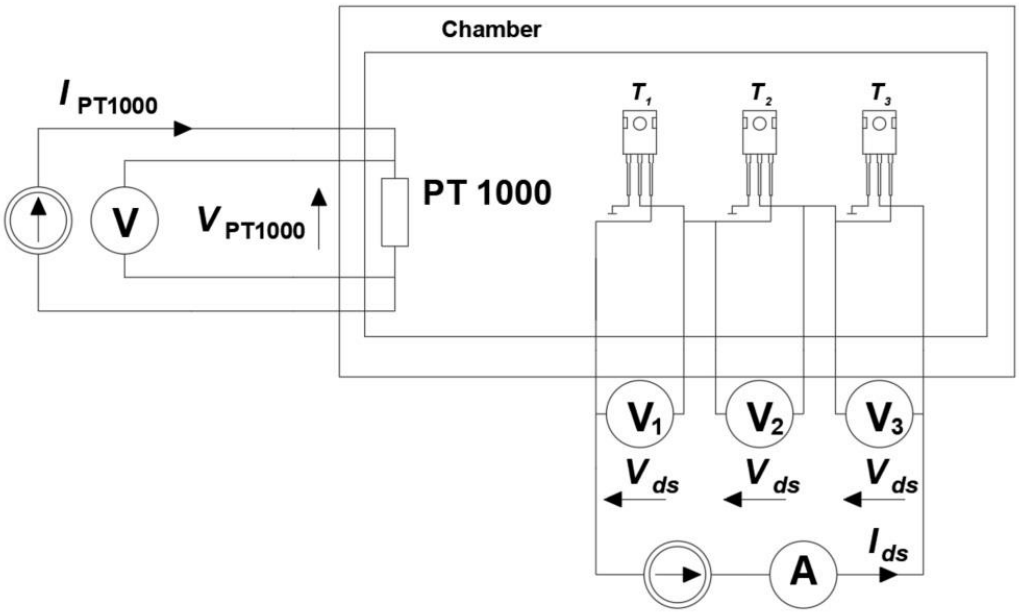

Figure 6. Measurement system enabling determination of the relationship $T_j = f(V_{fd})$.

2.3. Power Dissipated in Die and Ambient Conditions

The correct simulation work using Solidworks 2020 SP05 requires determining the power P that has been released in the die and defining the boundary condition. The power released in the die can be determined using Equation (1):

$$P = V_{DS} \cdot I_{DS} \tag{1}$$

where: P—power (in W) dissipated in the die, V_{DS}—drop voltage (in V) between drain and source, I_{DS}—current (in A) flowing between drain and source.

The V_{DS} and I_{DS} values were measured with measurement errors, which can be determined using the UT51 multimeter documentation (UNI-T, Dongguan City, China). Therefore, the p value will also be within the range defined by the measurement error limit ΔP, which can be determined from Equation (2):

$$\Delta P = V_{DS} \cdot \Delta I_{DS} + I_{DS} \cdot \Delta V_{DS} \tag{2}$$

where: ΔV_{DS}—limiting error of the V_{DS} value (in V), ΔI_{DS}—limiting error of the I_{DS} value (in A). The ΔI_{DS} and ΔV_{DS} values can be determined using the formulas in the UT51 user manual [40].

The increase in die temperature is related to the distribution of effective power, P_{RMS}, in the die. For this reason, the Equation (3) should be used:

$$P_{RMS} = \sqrt{\frac{1}{T_k} \int_{t_0}^{t_0+T_k} P^2(t) dt} \tag{3}$$

where: t_0—beginning of the period, T_k—duration of the period.

The P_{RMS} value is also within the range that is determined by the limiting error ΔP_{RMS}. The limits of the range determined by ΔP_{RMS} can be determined using Equation (2).

The temperature gradient in the radiative heat flux path between the transistor's die and the transistor's case can be determined using Equation (4):

$$J = -k \cdot \nabla \cdot T \tag{4}$$

where: J—radiative heat flux ($W \cdot m^{-2}$), ∇—Nabla operator.

Equation (4) can be written as Equation (5):

$$J = -k \cdot \frac{dT}{dx} \tag{5}$$

where: x—distance between the points where the temperature values of the die and diode case were measured (m), J—radiative heat flux ($W \cdot m^{-2}$).

In order to solve Equation (5), we need to separate the differentials that are on the right-hand side of the equation. Consequently, it is possible to integrate the equation on both sides. The constant of integration can be found using Equation (6):

$$\begin{array}{c} \text{for } x = 0 \rightarrow T = T_1 \\ \text{for } x = x_k \rightarrow T = T_2 \end{array} \tag{6}$$

where: x_k—end point of the analyzed heat flow path (m), T_1—temperature at the starting point of the analyzed heat flow path (K), T_2—temperature at the end point of the analyzed heat flow path (K).

Consequently, it is possible to determine Equation (7):

$$T_1 - T_2 = -\frac{P_C}{S \cdot k} \cdot x_k \tag{7}$$

where: P_c—total power (in W) applied to the wall, S—area (m^2) of the wall penetrated by J ($W \cdot m^{-2}$).

Determining the correct temperature distribution in the transistor's case (using Solidworks 2020 SP05 Software) requires determining the radiation coefficient h_r. The h_r coefficient defines the amount of thermal energy transferred to the environment by radiation per unit time, per unit area, and per unit temperature difference between the body radiating energy and the environment. The value of h_r can be determined using Equation (8):

$$h_r = \varepsilon \cdot \sigma \cdot (T_S \cdot T_a) \cdot \left(T_S^2 \cdot T_a^2 \right) \tag{8}$$

where: σ—Stefan–Boltzmann constant equal to 5.67×10^{-8} ($W \cdot m^{-2} \cdot K^{-4}$), T_S—surface temperature (K), T_a—air temperature (K).

It is also necessary to determine the value of the convection coefficient h_{cf}, which defines the amount of thermal energy transferred to the environment by convection per unit time, per unit area, and per unit temperature difference between the body emitting the energy and the environment. To determine the h_{cf} value for a flat surface, Equation (9) can be used:

$$h_{cf} = \frac{Nu \cdot k}{L} \tag{9}$$

where: h_{cf}—convection coefficient of flat surfaces, Nu—Nusselt number (-), L—characteristic length in meters (for a vertical wall, this value represents height).

The Nusselt number can be determined using Equation (10).

$$Nu = a \cdot (Pr \cdot Gr)^b \tag{10}$$

where: Gr—Grashof number (-), Pr—Prandtl number (-), a and b—dimensionless coefficients. The values of coefficients a and b are provided in Table 1.

Table 1. Values of coefficients a and b in Equation (10). lam—value for laminar flow, turb—value for turbulent flow.

Shape	$\boldsymbol{Gr \cdot Pr}$	$\boldsymbol{a_{lam}}$	$\boldsymbol{b_{lam}}$	$\boldsymbol{a_{turb}}$	$\boldsymbol{b_{turb}}$
Vertical flat wall	10^9	0.59	0.25	0.129	0.33
Upper flat wall	10^8	0.54	0.25	0.14	0.33
Lower flat wall	10^5	0.25	0.25	NA	NA

The Grashof number can be obtained from Equation (11):

$$Gr = \frac{\alpha \cdot g \cdot (T_s - T_a) \cdot \rho^2 \cdot L^3}{\eta^2} \tag{11}$$

where: g—gravitational acceleration ($9.8\ m \cdot s^{-2}$), α—coefficient of expansion ($0.0034\ K^{-1}$), ρ—air density ($1.21\ kg \cdot m^{-3}$) at 273.15 K, η—dynamic air viscosity ($1.75 \times 10^{-5}\ kg \cdot m^{-1} \cdot s^{-1}$) at 273.15 K.

Prandtl's number is determined from Equation (12):

$$Pr = \frac{c \cdot \eta}{k} \tag{12}$$

where: Pr—Prandtl's number, c—specific heat of air ($1005\ J \cdot kg^{-1} \cdot K^{-1}$) at 293.15 K.

When the value of the average linear velocity of the fluid flow is greater than 0 m/s, the Reynolds number must also be taken into account, which can be obtained using Equation (13):

$$Re = \frac{V \cdot \rho \cdot L}{\eta} \tag{13}$$

where: V—average linear velocity of the fluid flow (m/s).

In order to enable a better understanding of the boundary condition, the analyzed heat flow path and its emission by the observed surface (by convection h_{cf} and radiation h_r) are shown in Figure 7.

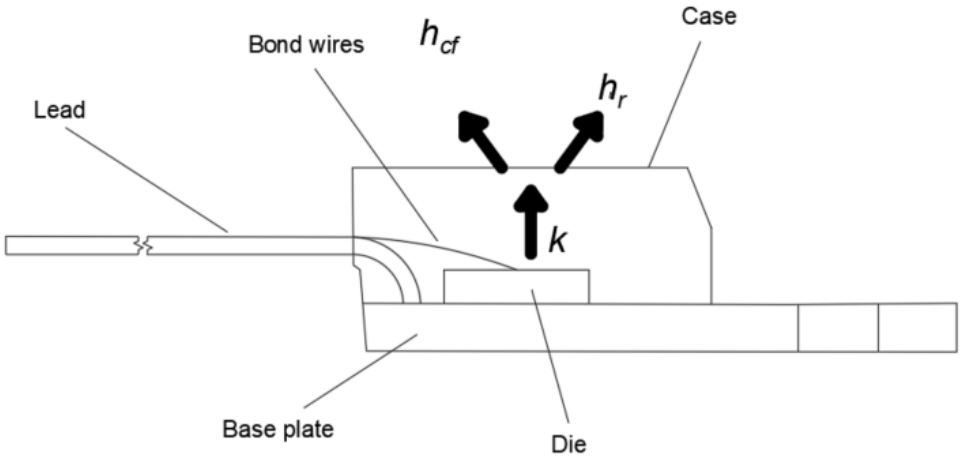

Figure 7. Analyzed heat flow path and its emission from the observed surface (by convection h_{cf} and radiation h_r). Thermal conductivity is designated as k.

2.4. Uncertainties

The method by which the uncertainty of the thermographic temperature measurement T_c can be determined is described in the document *Evaluation of the Uncertainty of Measurement in calibration* (EA-4/02 M: 2022) [41]. This is a method for determining the uncertainty of type B. In order to use this method, all input quantities X_i that affect the result of the T_c measurement and the range of their variability must be determined. This can be done based on experience and the literature. In this work, the thermographic camera processing equation from publication [42] was used (Equation (14)):

$$T_c = \sqrt[4]{\frac{T_{cam}^4 \cdot \varepsilon \cdot \sigma - (1-\varepsilon) \cdot \tau_a \cdot \sigma \cdot T_{refl}^4 \cdot \tau_l - (1-\tau_a) \cdot \sigma_c \cdot T_a^4 \cdot \tau_l - (1-\tau_l) \cdot \sigma_c \cdot T_l^4}{\varepsilon \cdot \tau_a \cdot \sigma_c \cdot \tau_l}} \quad (14)$$

where: T_{cam}—temperature indicated by the thermographic camera without taking into account the influence of other factors, σ_c—Stefan-Boltzmann constant equal to 5.67×10^{-8} ($W \cdot m^{-2} \cdot K^{-4}$), τ_a—atmosphere transmittance coefficient, τ_1—transmittance of the thermographic camera lens, T_a—air temperature, T_{refl}—reflected temperature, T_l—thermographic camera lens temperature.

The next step is to determine the sensitivity coefficient c_s for all input quantities from Equation (14). This is a derivative described in Equation (15):

$$c_s(y) = \frac{\partial f}{\partial X_i} \quad (15)$$

where: f_i—all input quantities from Equation (14).

In order to determine the uncertainty of the T_c value, estimates of x_i of the input quantities X_i (for all above input quantities) must be determined. This is possible using Equation (16) (rectangular probability distribution):

$$x_i = \frac{1}{2}(a_+ + a_-) \quad (16)$$

where: a_+—upper limit of the input quantity range, a_-—lower limit of the input quantity range.

Then, for each X_i, the uncertainty standard $u(x_i)$ should be determined as per Equation (17):

$$u^2(x_i) = \frac{1}{12}(a_+ - a_-)^2 \tag{17}$$

By multiplying the values of $u(x_i)$ and c_s, we can obtain the uncertainty contribution $u(y)$. The standard uncertainty $u(T_c)$ of the T_c value can be obtained as the square root of the sum of squares of the values of $u(y)$ as per Equation (18):

$$u^2(T_c) = \sum_{i=1}^{N} u(y) \tag{18}$$

In order to determine the expanded uncertainty $U(T_c)$, the value of $u(T_c)$ should be multiplied by the coverage factor k.

To determine $\Delta T_{\mathrm{Pt1000}}$, Equations (19)–(23) can be used:

$$\delta V_{\mathrm{Pt1000}} = \frac{\Delta V_{\mathrm{Pt1000}}}{V_{\mathrm{Pt1000}}} \cdot 100 \tag{19}$$

$$\delta I_{\mathrm{Pt1000}} = \frac{\Delta I_{\mathrm{Pt1000}}}{I_{\mathrm{Pt1000}}} \cdot 100 \tag{20}$$

$$\delta R_{\mathrm{Pt1000}} = \delta V_{\mathrm{Pt1000}} + \delta I_{\mathrm{Pt1000}} \tag{21}$$

$$\Delta R_{\mathrm{Pt1000}} = \frac{R_{\mathrm{Pt1000}} \cdot \delta R_{\mathrm{Pt1000}}}{100} \tag{22}$$

where: $\Delta V_{\mathrm{Pt1000}}$—limit error of V_{Pt1000}, $\delta V_{\mathrm{Pt1000}}$—relative error of V_{Pt1000}, $\Delta I_{\mathrm{Pt1000}}$—limit error of I_{Pt1000}, $\delta I_{\mathrm{Pt1000}}$—relative error of I_{Pt1000}, $\delta R_{\mathrm{Pt1000}}$—relative error of R_{Pt1000}, $\Delta R_{\mathrm{Pt1000}}$—limit error of R_{Pt1000}, R_{Pt1000}—resistance of Pt1000 [42].

Then, by inserting the upper and lower range of $\Delta R_{\mathrm{Pt1000}}$ into Equation (23), it is possible to obtain the upper and lower range of $\Delta T_{\mathrm{Pt1000}}$ values:

$$T_{\mathrm{Pt1000}} = 10^{-5} \cdot R_{\mathrm{Pt1000}}^2 + 0.235 \cdot R_{\mathrm{Pt1000}} - 245.35 + R_{\mathrm{Pt1000}}^2 \cdot 4 \cdot 10^{-7} - R_{\mathrm{Pt1000}} \cdot 2 \cdot 10^{-5} + 0.0011 \tag{23}$$

To determine the $\Delta V_{\mathrm{Pt1000}}$ and $\Delta I_{\mathrm{Pt1000}}$ values, the documentation of the multimeter describe in reference [40] can be used.

3. Results

Using the measurement system shown in Figure 6, the relationship $T_{jd} = f(V_{fd})$ was determined. This relationship was approximated by the linear equation $y = e \cdot x + f$. As a result, the individual equations $T_{jd} = T_C + e \cdot V_{fd} + f$ were obtained for each transistor. The values of the coefficients for each transistor are given in Table 2.

Table 2. Values of the coefficients e and f of the curves $T_{jd} = T_C + e \cdot V_{fd} + f$ of the tested transistors.

No	*Transistor*	*e*	*f*
1	C2M0280120D	8.9582	1.6507
2	C2M0280120D	8.9684	1.6012
3	C2M0280120D	8.9549	1.6577

Then, each of the tested transistors was connected according to the diagram shown in Figure 4. The black part of the transistor case was observed with a thermographic camera. In order to minimize the factors disturbing the thermographic measurements, the observed transistors and the thermographic camera were placed in a chamber whose connection layout is shown in Figure 3. Additionally, V_{fd} values were measured using a voltmeter. Using these values, the junction temperature T_{jd} values were determined based on the previously determined relationship $T_{jd} = f(V_{fd})$ (Table 2). The T_{jd} values determined in this way are given in Table 2, and sample recorded thermograms are shown in Figure 8.

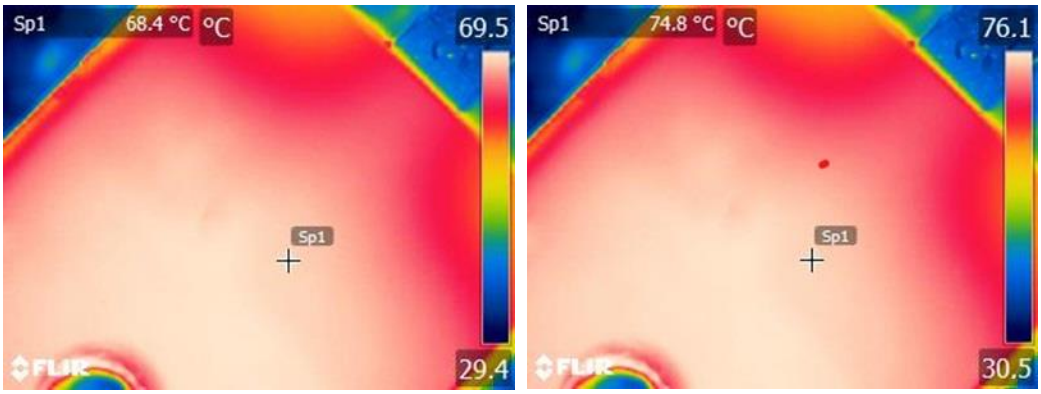

(**a**) (**b**)

Figure 8. Examples of recorded thermograms: (**a**) I_{DS} = 1 A; f_T = 1 kHz, (**b**) I_{DS} = 1 A; f_T = 10 kHz. The thermograms were taken before gluing the Pt1000.

In the next stage of the research, simulations were carried out using the FEM method. In the first step, a model of the tested transistor was designed. Materials and thermal conductivity values *k* are given in Table 3.

Table 3. Materials specified in the 3D model and their thermal conductivity values *k*.

Internal Structure Component	Material	*k* [W/m·K]
Black part of the case	EME 590	0.25
Back part of the case	Copper	400
Semiconductor element	Silicon carbide	150
Left lead	Copper	400
Internal lead	Copper	400
Right lead	Copper	400
Internal connections	Copper	400
Grease	Melamine resin	0.20

The selected values of the convection coefficients h_{cf} of the observed surface (black part of the case) were in the range of 15.3 W/m^2 K to 24.8 W/m^2 K for the tested temperature ranges.

Additionally, the relationship between the mesh size *l* specified in the simulation parameters, the duration of a single simulation t_s, and the accuracy of the determined temperature values DT_S was checked. The obtained results are presented in Table 4.

Table 4. Mesh size *l*, simulation duration t_s, and temperature values T_S obtained during FEM simulation defined in the simulation parameters.

No.	t_s [s]	*l* [mm]	ΔT_S [°C]
1	3	4.0	1.9
2	5	3.0	1.4
3	8	2.0	0.6
4	15	1.5	0.4
5	41	1.0	0.1
6	499	0.5	0.1

Based on the data presented in Table 4, a mesh size was selected at which the simulation duration was sufficiently short and the accuracy of the ΔT_S temperature value obtained as a result of the simulation work was 0.1 °C (Table 4, No. 5). As a result, the T_S temperature values obtained from the simulation work were close to the temperature T_c recorded in

the thermographic measurement for a given value of the power dissipated in the P_{RMS} transistor. The selected mesh size was l = 1.0 mm. The example temperature distributions obtained from the simulation are shown in Figure 9.

Tables 5–8 present the values of T_c and T_j recorded during measurements and the values of T_S (transistor case) obtained as a result of simulation work, depending on the set value of the switching frequency f_T of the transistor. The measurements were carried out for four current values.

In order to determine the uncertainty of the T_c value, the range of all variables was determined from Equation (14). The adopted ranges of values and the determined x_i are given in Table 9.

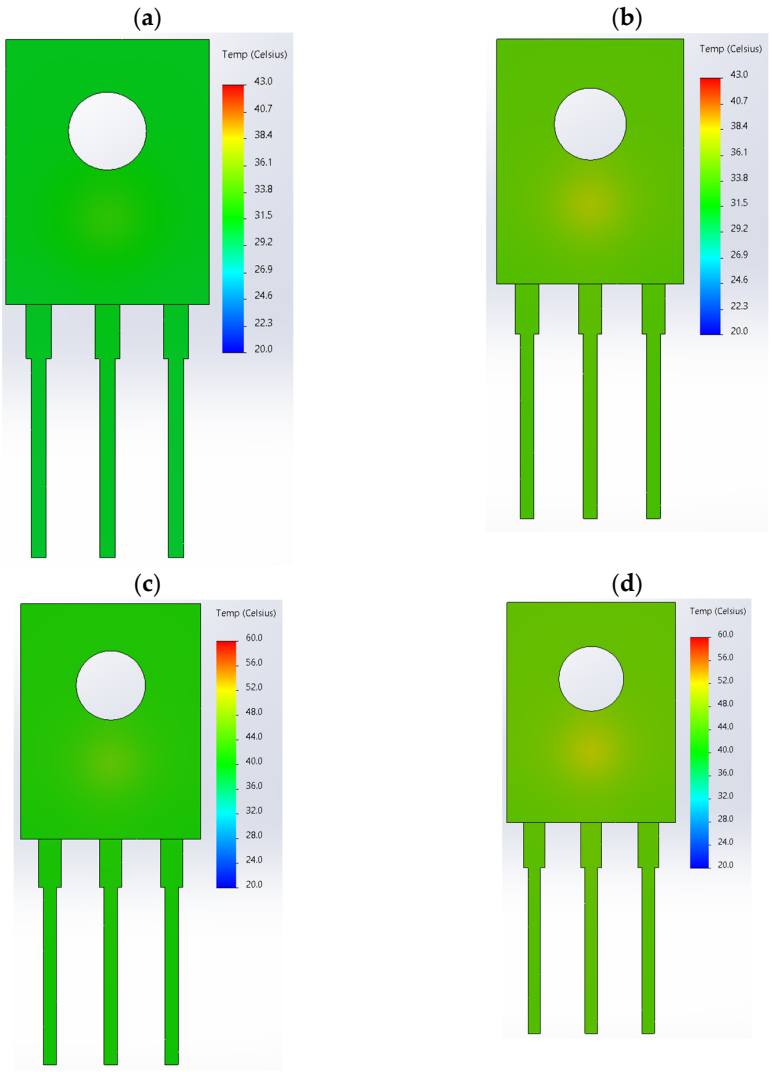

Figure 9. *Cont.*

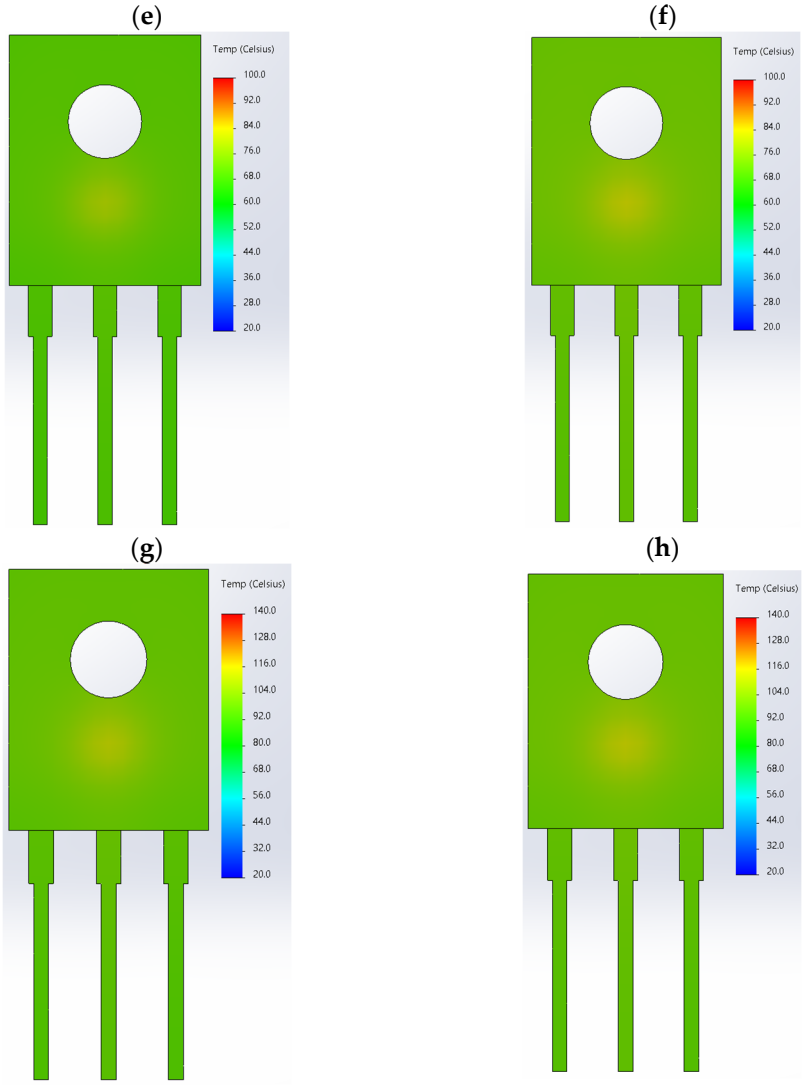

Figure 9. Examples of temperature distributions obtained from FEM simulations. (**a**) I_{DS} = 0.25 A, f_T = 1 kHz, (**b**) I_{DS} = 0.25 A, f_T = 500 kHz, (**c**) I_{DS} = 0.5 A, f_T = 1 kHz, (**d**) I_{DS} = 0.5 A, f_T = 500 kHz, (**e**) I_{DS} = 1 A, f_T = 1 kHz, (**f**) I_{DS} = 1 A, f_T = 500 kHz, (**g**) I_{DS} = 1.5A, f_T = 1 kHz, (**h**) I_{DS} = 1.5A, f_T = 500 kHz.

Table 5. Transistor case temperature T_c determined from thermographic measurements, junction temperature T_{jd} determined from the relationship $T_{jd} = f(V_{fd})$, and transistor case temperature T_S and junction temperature T_j determined from simulations, depending on the set switching frequency f_T. The results were obtained for the current I_{DSmax} = 0.25 A. T_{c1} is the T_c value measured for the first transistor, T_{c2} is the T_c value measured for the second transistor, and T_{c3} is the T_c value measured for the third transistor.

No.	f_T [kHz]	I_{DS} [A]	P [W]	T_{c1} [°C]	T_{c2} [°C]	T_{c3} [°C]	T_{jd} [°C]	T_S [°C]	T_j [°C]	T_{Pt1000} [°C]
1	1	0.25	0.52	33.1	33.3	32.6	53.4	33.0	49.4	31.1
2	5	0.25	0.52	33.4	33.6	32.9	53.7	33.3	49.8	31.4
3	10	0.25	0.52	33.6	33.8	33.1	53.9	33.5	50.1	31.6
4	50	0.25	0.52	33.9	34.2	33.3	54.2	33.8	50.5	31.9
5	100	0.25	0.52	34.3	34.6	33.7	54.6	34.2	51.1	32.3
6	150	0.25	0.52	35.0	35.3	34.4	55.3	34.9	52.1	32.9
7	200	0.25	0.52	35.6	35.9	35.0	55.9	35.5	53.1	33.6
8	300	0.25	0.52	36.6	36.9	36.0	56.9	36.5	54.2	34.6
9	400	0.25	0.52	36.9	37.2	36.3	57.2	36.8	54.9	34.9

Table 5. *Cont.*

No.	f_T [kHz]	I_{DS} [A]	P [W]	T_{c1} [°C]	T_{c2} [°C]	T_{c3} [°C]	T_{jd} [°C]	T_S [°C]	T_j [°C]	T_{Pt1000} [°C]
10	500	0.25	0.52	37.3	37.6	36.7	57.5	37.2	55.5	35.3
11	600	0.25	0.52	37.1	37.4	36.5	57.3	37.0	55.1	35.1
12	700	0.25	0.52	37.3	37.6	36.7	57.5	37.2	55.3	35.3
13	800	0.25	0.52	37.6	37.9	37.0	57.8	37.5	55.7	35.6

Table 6. Transistor case temperature T_c determined from the thermographic measurements, junction temperature T_{jd} determined from the relationship $T_{jd} = f(V_{fd})$, and the transistor case temperature T_S and junction temperature T_j determined from simulations, depending on the set switching frequency f_T. The results were obtained for the current I_{DSmax} = 0.5 A. T_{c1} is the T_c value measured for the first transistor, T_{c2} is the T_c value measured for the second transistor, T_{c3} is the T_c value measured for the third transistor.

No.	f_T [kHz]	I_{DS} [A]	P [W]	T_{c1} [°C]	T_{c2} [°C]	T_{c3} [°C]	T_{jd} [°C]	T_S [°C]	T_j [°C]	T_{Pt1000} [°C]
1	1	0.5	1.20	45.7	46.1	45.3	68.8	45.7	66.3	43.7
2	5	0.5	1.19	45.7	46.1	45.3	68.7	45.7	66.3	43.7
3	10	0.5	1.19	46.0	46.4	45.6	69.0	46.0	66.7	44.0
4	50	0.5	1.18	47.0	47.4	46.6	69.8	47.0	67.2	45.0
5	100	0.5	1.18	48.1	48.5	47.7	70.8	48.1	68.7	46.1
6	150	0.5	1.17	49.2	49.6	48.8	71.8	49.2	69.3	47.2
7	200	0.5	1.17	50.1	50.5	49.7	72.7	50.1	70.7	48.0
8	300	0.5	1.17	50.9	51.3	50.5	73.5	50.9	71.9	48.8
9	400	0.5	1.17	50.7	51.1	50.3	73.3	50.7	71.6	48.6
10	500	0.5	1.17	51.0	51.4	50.6	73.5	51.0	71.1	48.9
11	600	0.5	1.17	51.6	52.0	51.2	74.1	51.6	72.0	49.5
12	700	0.5	1.17	51.5	51.9	51.1	74.0	51.5	71.8	49.4
13	800	0.5	1.16	51.3	51.7	50.9	73.8	51.3	71.5	49.2

Table 7. Transistor case temperature T_c determined from thermographic measurements, junction temperature T_{jd} determined from the relationship $T_{jd} = f(V_{fd})$, and transistor case temperature T_S and junction temperature T_j determined from simulations, depending on the set switching frequency f_T. The results were obtained for the current I_{DSmax} = 1 A. T_{c1} is the Tc value measured for the first transistor, T_{c2} is the Tc value measured for the second transistor, T_{c3} is the T_c value measured for the third transistor.

No.	f_T [kHz]	I_{DS} [A]	P [W]	T_{c1} [°C]	T_{c2} [°C]	T_{c3} [°C]	T_{jd} [°C]	T_S [°C]	T_j [°C]	T_{Pt1000} [°C]
1	1	1	2.90	80.0	80.6	79.7	107.7	80.1	106.1	77.8
2	5	1	2.90	80.4	81.0	80.1	108.1	80.5	106.3	78.2
3	10	1	2.89	79.9	80.5	79.6	107.6	80.0	106.1	77.7
4	50	1	2.88	81.6	82.2	81.3	109.1	81.7	106.6	79.4
5	100	1	2.87	81.9	82.5	81.6	109.4	82.0	106.8	79.7
6	150	1	2.86	81.7	82.3	81.4	109.1	81.8	106.5	79.5
7	200	1	2.86	82.4	83.0	82.1	109.8	82.5	106.8	80.1
8	300	1	2.85	83.0	83.6	82.7	110.3	83.1	106.8	80.7
9	400	1	2.85	83.1	83.7	82.8	110.4	83.2	106.9	80.8
10	500	1	2.85	83.1	83.7	82.8	110.4	83.2	106.9	80.8
11	600	1	2.85	82.9	83.5	82.6	110.1	83.0	106.7	80.6
12	700	1	2.85	83.1	83.7	82.8	110.3	83.2	106.7	80.8
13	800	1	2.85	83.0	83.6	82.7	110.2	83.1	106.6	80.7

Table 8. Transistor case temperature T_c determined from thermographic measurements, junction temperature T_{jd} determined from the relationship $T_{jd} = f(V_{fd})$, and transistor case temperature T_S and junction temperature T_j determined from simulations, depending on the set switching frequency f_T. The results were obtained for the current I_{DSmax} = 1.5 A. T_{c1} is the T_c value measured for the first transistor, T_{c2} is the T_c value measured for the second transistor, T_{c3} is the T_c value measured for the third transistor.

No.	f_T [kHz]	I_{DS} [A]	P [W]	T_{c1} [°C]	T_{c2} [°C]	T_{c3} [°C]	T_{jd} [°C]	T_S [°C]	T_j [°C]	T_{Pt1000} [°C]
1	1	1.5	3.30	111.9	112.6	111.8	141.9	112.1	140.0	109.5
2	5	1.5	3.29	113.3	114.0	113.2	143.2	113.5	140.7	110.8
3	10	1.5	3.28	113.4	114.1	113.3	143.2	113.6	140.9	110.9
4	50	1.5	3.27	113.2	113.9	113.1	142.9	113.4	140.5	110.7
5	100	1.5	3.26	113.3	114.0	113.2	142.9	113.5	140.7	110.8
6	150	1.5	3.25	113.4	114.1	113.3	143.0	113.6	140.9	110.9
7	200	1.5	3.24	113.3	114.0	113.2	142.8	113.5	140.7	110.8
8	300	1.5	3.22	113.4	114.1	113.3	142.7	113.6	140.9	110.9
9	400	1.5	3.22	113.4	114.1	113.3	142.7	113.6	140.9	110.9
10	500	1.5	3.22	113.4	114.1	113.3	142.7	113.6	140.9	110.9
11	600	1.5	3.22	113.3	114.0	113.2	142.6	113.5	140.7	110.8
12	700	1.5	3.22	113.4	114.1	113.3	142.7	113.6	140.9	110.9
13	800	1.5	3.22	113.4	114.1	113.3	142.7	113.6	140.9	110.9

Table 9. Values of the variables from Equation (14) and the determined x_i.

No	Value	Unit	a_+	a_-	x_i
1	ε	-	0.98	0.96	0.97
2	τ_a	-	1.00	0.98	0.99
3	T_{refl}	°C	5.00	0.00	2.50
4	τ_l	-	1.00	0.98	0.99
5	T_a	°C	30.00	16.00	22.5
6	T_l	°C	30.00	16.00	22.5

The T_{cam} value was also taken into account. The T_{cam} value limits were selected individually for each case ($T_{cam} \pm 2$ °C).

Then, using equations from Section 2.4, the standard uncertainty $u(x_i)$ and sensitivity coefficient c_s (for all input quantities from Equation (14)) were determined. For each X_i, the uncertainty contribution $u(y)$ was determined. The T_{cam} value was added to the budget with c_s equal to 1. After constructing the uncertainty budget, the standard uncertainty $u(T_c)$ was determined. An example uncertainty budget for f_t = 1 kHz and I_{DS} = 0.25 A. T_{cc} = 304.3 °C is shown in Table 10.

The value of $U(T_c)$ = 2.36 °C was obtained by multiplying the value of 1.18 by k = 2. Using the formulas presented in Section 2.4, the maximum value of ΔT_{Pt1000} of 1.73 °C was also determined.

Table 10. Example uncertainty budget for f_t = 1 kHz and I_{DS} = 1.5 A T_{c1} = 112.1 °C.

Symbol	Unit	x_i	$u(x_i)$	Probability Distribution	c_s	$u_i(y)$
τ_a	-	0.99	0.01	normal	0.45	0.01
ε	-	0.95	0.03	rectangular	−7.65	−0.22
T_{refl}	°C	20.85	1.44	rectangular	0.01	0.02
τ_l	-	0.99	0.01	rectangular	−10.32	−0.06
T_a	°C	20.85	4.04	rectangular	−0.02	−0.06
T_l	°C	20.85	4.04	rectangular	−0.02	−0.06
T_{cam}	°C	20.85	1.15	rectangular	1.00	1.15
T_c	°C	112.1				1.18

4. Discussion

During the experimental work, an additional lens (Close-up 2×) was used with the thermographic camera. This enabled the thermographic camera used during the measurements (equipped with a 240 × 180 pixels detector matrix) to obtain such spatial resolution for which the edge of the field of view of a single detector was 67 µm. This value, taking into account the dimensions of the transistor shown in Figure 2, guaranteed that 25 fields of the view of a single detector of the thermographic camera (fields of the view placed in a rectangle of 5 × 5 pixels) were placed on the transistor case during the measurement. For this reason, the result of the thermographic temperature measurement can be considered reliable.

Before starting the measurements, the performance of the thermographic camera was compared with to the IRS Calilux radiation standard (Automation Technology, Bad Oldesloe, Germany). The results were compared in the range of 30–90 °C with a step of 5 °C. The largest difference between the standard and the camera was 0.72 °C (the camera error was ±2 °C or ±2%, whichever is greater). For this reason, the output from the thermographic camera can be considered reliable.

The results of the thermographic temperature measurements were comparable to those obtained using the Pt1000 sensor and to the results obtained during simulation work using the FEM method. During the work carried out, three transistor specimens were tested. Similar measurement results were obtained for each. Brand new Pt1000 sensors were used.

Analyzing the data from Tables 5–8 (and especially comparing the die temperature (T_j) determined based on the simulation and the voltage drop T_{jd}) it can be seen that the largest difference was 4 °C. The conducted studies prove that the use of the transistor body diode during measurements allows for obtaining reliable results. They also prove that the results obtained by simulation work are confirmed in real conditions. Comparing the case temperature determined by simulation work (T_S) with the temperature measured by means of a thermographic camera (T_c), it can be seen that these values are the same. This proves that the model created is reliable.

Analyzing the data from Tables 5–8, it can be seen that the difference between all results for T_{c1}–T_{c3} are within the limit defined by the uncertainty $U(T_c)$. It can also be seen that the values of T_{c1}–T_{c3} and T_S and T_{Pt1000} are within the range defined by $\Delta T_{\mathrm{Pt1000}}$ and $U(T_c)$. For this reason, it can be assumed that the thermographic temperature measurement is reliable.

5. Conclusions

The aim of this research was to develop a method for performing indirect thermographic measurement of a SiC MOSFET and monitoring the SiC MOSFET temperature at variable switching frequencies.

Analyzing the transistor case temperatures measured with a thermographic camera (T_c) at a frequency f_t, it can be seen that despite the constant value of the I_{DS} current, the T_c value increases. The increase in the T_c value depends on the I_{DS} value. For the value of I_{DS} = 0.25 A and f_t in the range of 1 kHz–800 kHz, the T_c value increased by 4.5 °C. For the value of I_{DS} = 0.5 A and f_t in the range of 1 kHz–800 kHz, the T_c value increased by 5.6 °C. For the value of I_{DS} = 1 A and f_t in the range of 1 kHz–800 kHz, the T_c value increased by 3 °C. For the value of I_{DS} = 1.5 A and f_t in the range of 1 kHz–800 kHz, the T_c value increased by 1.5 °C. The T_c value depends on the value of I_{DS} and f_t. With the increase in I_{DS}, the T_c value is set at increasingly lower values of f_T.

The largest recorded difference between the case temperature and the die temperature was 27.3 °C. The use of a thermographic camera allows determining the temperature of the transistor die, which allows selecting the optimal control of the C2M0280120D transistor.

Due to the use of thermographic, there is no risk of electric shock as a result of touching the base plate or radiator, and the measurement result is obtained immediately. Based on a properly performed thermographic measurement of the temperature of the black part

of the case (made of epoxy mold compound), it is possible to determine the temperature of the transistor die. As a result, its optimal operating point can be selected even more precisely. It is also possible to capture the operating point at which the transistor begins to operate incorrectly. This will prevent damage and save funds that would have to be spent in the event of a failure.

Author Contributions: Conceptualization, K.D.; methodology, K.D. and A.H.; formal analysis, K.D., A.H. and Ł.D.; investigation, K.D. and A.H.; resources, K.D.; writing—original draft preparation, K.D., A.H. and Ł.D.; writing—review and editing, K.D., A.H. and Ł.D.; visualization, K.D.; supervision, K.D. and A.H. All authors have read and agreed to the published version of the manuscript.

Funding: This research was funded by the Ministry of Science and Higher Education, grant numbers 0212/SBAD/0617 and 0212/SBAD/0618.

Institutional Review Board Statement: Not applicable.

Informed Consent Statement: Not applicable.

Data Availability Statement: Data are contained within the article.

Conflicts of Interest: The authors declare no conflicts of interest.

Nomenclature

a and b	dimensionless coefficients
a_+	upper limit of the input quantity range
a_-	lower limit of the input quantity range
a_{lam}	value of coefficient a for laminar flow
b_{lam}	value of coefficient b for laminar flow
a_{turb}	value of coefficient a for turbulent flow
b_{turb}	value of coefficient b for turbulent flow
c	specific heat of air equal to 1005 $J \cdot kg^{-1} \cdot K^{-1}$ at 293.15 K
c_s	sensitivity coefficient
d	distance between the tested transistor and the additional lens
DUT	device under test
e	slope of the equation T_{jd} = f(V_{fd}) of the transistor
f	free term of the equation T_{jd} = f(V_{fd}) of the transistor
FEM	finite element method
f_i	all input quantities from Equation (14)
f_T	switching frequency
g	gravitational acceleration (9.8 $m \cdot s^{-2}$)
Gr	Grashof number
h_{cf}	convection coefficient of flat surfaces
h_r	radiation coefficient
I_D	drain current
I_{DS}	drain—source current (in A)
I_{Dpulse}	pulse current
I_{Pt1000}	current flowing through Pt1000
IFOV	instantaneous field of view
IR	infrared radiation
J	radiative heat flux
K	thermal conductivity
k	coverage factor
L	characteristic length in meters (for a vertical wall, this value represents height)
Nu	Nusselt number
P_{RMS}	power supplied to the transistor
P	power dissipated in the die (in W)
P_c	total power applied to the wall
Pr	Prandtl number
Re	Reynolds number
R_{Pt1000}	resistance of Pt1000

S	area of the wall penetrated by J
T_a	ambient temperature
T_c	case temperature
T_{c1}	T_c value measured for the first transistor
T_{c2}	T_c value measured for the second transistor
T_{c3}	T_c value measured for the third transistor
T_{cam}	temperature indicated by the thermographic camera
T_k	duration of the period
T_j	junction temperature
T_d	junction temperature determined electrically
T_l	thermographic camera lens temperature
T_{Pt1000}	temperature value measured with Pt1000
T_{refl}	reflected temperature
T_1	temperature at the starting point of the analyzed heat flow path (K)
T_2	temperature at the end point of the analyzed heat flow path (K)
t_0	beginning of the period
$u(x_i)$	standard uncertainty of each X_i,
$u(y)$	uncertainty contribution
$u(T_c)$	standard uncertainty of T_c values
$U(T_c)$	expanded uncertainty of T_c values
V	average linear velocity of the fluid flow
V_{DS}	drop voltage between drain and source (in V)
V_{Dsmax}	maximum drain—source voltage
V_{fd}	diode forward voltage
V_{GS}	gate—source voltage
V_{GSmax}	maximum gate—source voltage
V_{Pt1000}	voltage drop on Pt1000
x	distance between the points where the temperature values of the die and diode case were measured, and J is the radiative heat flux
x_k	end point of the analyzed heat flow path
X_i	input quantities
x_i	estimates of the input quantities X_i
∇	Nabla operator
α	coefficient of expansion equal to 0.0034 K^{-1}
ε	emissivity factor
ΔI_{DS}	limiting error of the I_{DS} value (in A)
ΔV_{DS}	limiting error of the V_{DS} value (in V)
$\Delta I_{\mathrm{Pt1000}}$	limit error of I_{Pt1000}
$\delta I_{\mathrm{Pt1000}}$	relative error of I_{Pt1000}
ΔP	limiting error of the P value in W
$\delta R_{\mathrm{Pt1000}}$	relative error of R_{Pt1000}
$\Delta R_{\mathrm{Pt1000}}$	limit error of R_{Pt1000}
$\Delta T_{\mathrm{Pt1000}}$	limit error of $\Delta T_{\mathrm{Pt1000}}$ of measurement T_{Pt1000}
$\Delta V_{\mathrm{Pt1000}}$	limit error of V_{Pt1000}
$\delta V_{\mathrm{Pt1000}}$	relative error of V_{Pt1000}
η	dynamic air viscosity equal to 1.75×10^{-5} $\mathrm{kg \cdot m^{-1} \cdot s^{-1}}$ at 273.15 K
ρ	density equal to 1.21 ($\mathrm{kg \cdot m^{-3}}$) in 273.15 (K)
σ_c	Stefan–Boltzmann constant
τ_a	atmosphere transmittance coefficient
τ_l	transmittance of the thermographic camera lens

References

1. Božanić, M.; Sinha, S. Emerging Transistor Technologies Capable of Terahertz Amplification: A Way to Re-Engineer Terahertz Radar Sensors. *Sensors* **2019**, *19*, 2454. [CrossRef]
2. Ibrahim, M.S.; Abbas, W.; Waseem, M.; Lu, C.; Lee, H.H.; Fan, J.; Loo, K.-H. Long-Term Lifetime Prediction of Power MOSFET Devices Based on LSTM and GRU Algorithms. *Mathematics* **2023**, *11*, 3283. [CrossRef]
3. Dziarski, K.; Hulewicz, A.; Kuwałek, P.; Wiczyński, G. Methods of Measurement of Die Temperature of Semiconductor Elements: A Review. *Energies* **2023**, *16*, 2559. [CrossRef]

4. Ulrich, R.K.; Brown, W.D. *Advanced Electronic Packaging*; Wiley-IEEE Press: Hoboken, NJ, USA, 2006.
5. Wang, Y.; Ding, Y.; Yin, Y. Reliability of Wide Band Gap Power Electronic Semiconductor and Packaging: A Review. *Energies* **2022**, *15*, 6670. [CrossRef]
6. Millan, J. Wide band-gap power semiconductor devices. *IET Circuits Devices Syst.* **2007**, *1*, 372–379. [CrossRef]
7. Roussel, P. SiC Market and Industry Update. In Proceedings of the International SiC Power Electronics Application Workshop, Birmingham, UK, 1–2 September 2011; pp. 3–4.
8. Yang, X.; Xu, M.; Li, Q.; Wang, Z.; He, M. Analytical method for RC snubber optimization design to eliminate switching oscillations of SiC MOSFET. *IEEE Trans. Power Electron.* **2022**, *37*, 4672–4684. [CrossRef]
9. Gupta, A.; Ayyanar, R.; Chakraborty, S. Novel electric vehicle traction architecture with 48 V Battery and multi-input, high conversion ratio converter for high and variable DC-link voltage. *IEEE Open J. Veh. Technol.* **2021**, *2*, 448–470. [CrossRef]
10. Fabre, J.; Ladoux, P. Parallel connection of SiC MOSFET modules for future use in traction converters. In Proceedings of the 2015 International Conference on Electrical Systems for Aircraft, Railway, Ship Propulsion and Road Vehicles (ESARS), Aachen, Germany, 3–5 March 2015; pp. 1–6. [CrossRef]
11. Lagier, T.; Ladoux, P.; Dworakowski, P. Potential of silicon carbide MOSFETs in the DC/DC converters for future HVDC offshore wind farms. *High Volt.* **2017**, *2*, 233–243. [CrossRef]
12. Ding, X.; Lu, P.; Shan, Z. A high-accuracy switching loss model of SiC MOSFETs in a motor drive for electric vehicles. *Appl. Energy* **2021**, *291*, 116827. [CrossRef]
13. Scognamillo, C.; Catalano, A.P.; Riccio, M.; d'Alessandro, V.; Codecasa, L.; Borghese, A.; Tripathi, R.N.; Castellazzi, A.; Breglio, G.; Irace, A. Compact Modeling of a 3.3 kV SiC MOSFET Power Module for Detailed Circuit-Level Electrothermal Simulations Including Parasitics. *Energies* **2021**, *14*, 4683. [CrossRef]
14. Chen, M.; Wang, H.; Pan, D.; Wang, X.; Blaabjerg, F. Thermal characterization of silicon carbide MOSFET module suitable for high-temperature computationally efficient thermal-profile prediction. *IEEE J. Emerg. Sel. Top. Power Electron.* **2020**, *9*, 3947–3958. [CrossRef]
15. Du, H.; Reigosa, P.; Ceccarelli, L.; Iannuzzo, F. Impact of repetitive short-circuit tests on the normal operation of SiC MOSFETs considering case temperature influence. *IEEE J. Emerg. Sel. Topics Power Electron.* **2020**, *8*, 195–205. [CrossRef]
16. Tanimoto, S.; Ohashi, H. Reliability issues of SiC power MOSFETs toward high junction temperature operation. *Phys. Status Solidi A* **2019**, *206*, 2417–2430. [CrossRef]
17. Wang, H. Transitioning to physics-of-failure as a reliability driver in power electronics. *IEEE J. Emerg. Sel. Top. Power Electron.* **2014**, *2*, 97–114. [CrossRef]
18. Wang, H.; Liserre, M.; Blaabjerg, F. Toward reliable power electronics: Challenges design tools and opportunities. *IEEE Ind. Electron. Mag.* **2013**, *7*, 17–26. [CrossRef]
19. Li, H.; Liao, X.; Hu, Y.; Zeng, Z.; Song, E.; Xiao, H. Analysis of SiC MOSFET dI/dt and its temperature dependence. *IET Power Electron.* **2017**, *11*, 491–500. [CrossRef]
20. Yodwong, B.; Guilbert, D.; Kaewmanee, W.; Phattanasak, M. Energy Efficiency Based Control Strategy of a Three-Level Interleaved DC-DC Buck Converter Supplying a Proton Exchange Membrane Electrolyzer. *Electronics* **2019**, *8*, 933. [CrossRef]
21. Faizan, M.; Wang, X.; Yousaf, M.Z. Design and Comparative Analysis of an Ultra-Highly Efficient, Compact Half-Bridge LLC Resonant GaN Converter for Low-Power Applications. *Electronics* **2023**, *12*, 2850. [CrossRef]
22. Urkin, T.; Peretz, M.M. Asymmetrically Driven HB-LLC Resonant Converter Integrated in Low-Power IoT Devices. In Proceedings of the 2023 IEEE Applied Power Electronics Conference and Exposition (APEC), Orlando, FL, USA, 19–23 March 2023; pp. 2105–2110. [CrossRef]
23. Li, X.; Zhang, L.; Guo, S.; Lei, Y.; Huang, A.; Zhang, B. Understanding switching losses in SiC MOSFET: Toward lossless switching. In Proceedings of the 2015 IEEE 3rd Workshop on Wide Bandgap Power Devices and Applications (WiPDA), Blacksburg, VA, USA, 2–4 November 2015; pp. 257–262. [CrossRef]
24. Dziarski, K.; Hulewicz, A.; Drużyński, Ł.; Dombek, G. Indirect Thermographic Temperature Measurement of a Power-Rectifying Diode Die Based on a Heat Sink Thermogram. *Energies* **2023**, *16*, 332. [CrossRef]
25. JESD 51-53. Available online: https://www.jedec.org (accessed on 3 February 2024).
26. Bercu, N.; Lazar, M.; Simonetti, O.; Adam, P.M.; Brouillard, M.; Giraudet, L. KPFM-Raman Spectroscopy Coupled Technique for the Characterization of Wide Bandgap Semiconductor Devices. *Mater. Sci. Forum* **2022**, *1062*, 330–334. [CrossRef]
27. Avenas, Y.; Dupont, L.; Khatir, Z. Temperature measurement of power semiconductor devices by thermo-sensitive electrical parameters—A review. *IEEE Trans. Power Electron.* **2011**, *27*, 3081–3092. [CrossRef]
28. Abad, B.; Borca-Tasciuc, D.A.; Martin-Gonzalez, M.S. Non-contact methods for thermal properties measurement. *Renew. Sustain. Energy Rev.* **2017**, *76*, 1348–1370. [CrossRef]
29. Hulewicz, A.; Dziarski, K.; Drużyński, Ł.; Dombek, G. Thermogram Based Indirect Thermographic Temperature Measurement of Reactive Power Compensation Capacitors. *Energies* **2023**, *16*, 2164. [CrossRef]
30. Pt_1000. Available online: https://www.reichelt.com/ch/pl/czujnik-temperatury-p-lstrok-ytek-smd-0603-1000-om-oacute-w-smd-0603-pt1000-p151239.html?CCOUNTRY=459&LANGUAGE=fr&GROUPID=9145&START=0&OFFSET=16&SID=964d99ec818539c8448982376b9e52e375c224e23ed7359cb8a59&LANGUAGE=PL&&r=1 (accessed on 15 February 2024).
31. WLK 5. Available online: https://www.tme.eu/en/details/wlk_5/heatsinks-equipment/fischer-elektronik/wlk-5/ (accessed on 15 February 2024).

32. Kawor, E.T.; Mattei, S. Emissivity measurements for nexel velvet coating 811-21 between—36 °C and 82 °C. *High Temp.—High Press.* **2001**, *33*, 551–556. [CrossRef]
33. Flir E50. Available online: https://docs.rs-online.com/ca3e/0900766b81371810.pdf (accessed on 15 February 2024).
34. Close-up 2x (50 µm) T197214. Available online: https://www.ideadigitalcontent.com/files/12228/T197214-en-US_A4.pdf (accessed on 15 February 2024).
35. IRS Calilux. Available online: https://www.ndt.net/news/files/AT_Newsletter_3._Quarter_2020_ENG.pdf (accessed on 15 February 2024).
36. Krawiec, P.; Różański, L.; Czarnecka-Komorowska, D.; Warguła, Ł. Evaluation of the Thermal Stability and Surface Characteristics of Thermoplastic Polyurethane V-Belt. *Materials* **2020**, *13*, 1502. [CrossRef] [PubMed]
37. Siemens s71200 PLC. Available online: https://support.industry.siemens.com/cs/mdm/91696622?c=60698891275&dl=sk&lc=pl-pl (accessed on 15 February 2024).
38. Dziarski, K.; Hulewicz, A.; Drużyński, Ł.; Dombek, G. Indirect Thermographic Temperature Measurement of a Power Rectifying Diode Die under Forced Convection Conditions. *Appl. Sci.* **2023**, *13*, 4440. [CrossRef]
39. Agilent. Available online: https://www.agilent.com/?gad_source=1&gclid=CjwKCAjwm_SzBhAsEiwAXE2CvxfrIFaUKFw_i-uOUtxsLtOrH-DNMHQtVQQRM37HcCh6fHAZMqL4qxoCYOQQAvD_BwE&gclsrc=aw.ds (accessed on 16 March 2024).
40. UT55. Available online: https://www.uni-trend.com/ (accessed on 16 March 2024).
41. Available online: https://www.enac.es/documents/7020/635abf3f-262a-4b3b-952f-10336cdfae9e (accessed on 30 July 2024).
42. Dziarski, K.; Hulewicz, A.; Dombek, G. Lack of thermogram sharpness as component of thermographic temperature measurement uncertainty budget. *Sensors* **2021**, *21*, 4013. [CrossRef]